Miyazaki et al. Earth, Planets and Space (2015) 67:179
DOI 10.1186/s40623-015-0346-4

Earth, Planets and Space
a SpringerOpen Journal

LETTER Open Access

Triggered tremors beneath the seismogenic zone of an active fault zone, Kyushu, Japan

Masahiro Miyazaki*, Satoshi Matsumoto and Hiroshi Shimizu

Abstract

Non-volcanic tremors were induced by the surface waves of the 2012 Sumatra earthquake around the Hinagu fault zone in Kyushu, Japan. We inferred from dense seismic observation data that the hypocenters of these tremors were located beneath the seismogenic zone of the Hinagu fault. Focal mechanisms of the tremors were estimated using S-wave polarization angles. The estimated focal mechanisms show similarities to those of shallow earthquakes in this region. In addition, one of the nodal planes of the focal mechanisms is almost parallel to the strike direction of the Hinagu fault. These observations suggest that the tremors were triggered at the deeper extension of the active fault zone under stress conditions similar to those in the shallower seismogenic region. A low-velocity anomaly beneath the hypocentral area of the tremors might be related to the tremor activity.

Keywords: Triggered tremor, The Hinagu fault zone, Intraplate earthquake, Focal mechanism, Polarization analysis, Slow earthquake

Findings

Introduction

Non-volcanic tremors triggered by surface waves from teleseismic events have been detected all over the world. Most studies have investigated tremors that were located near or on plate boundaries such as subduction zones (Miyazawa and Brodsky 2008; Rubinstein et al. 2009; Yabe and Ide 2013), transform boundary zones (Peng et al. 2009), and collision zones (Chao et al. 2012). However, non-volcanic tremors are rarely detected away from plate boundaries. Obara (2012) found that triggered tremors occurred near a volcano and an active fault zone in Hokkaido, Japan and Kita et al. (2014) showed through analysis of seismic attenuation that such tremors occurred in a collision zone.

According to previous studies, most non-volcanic tremors occur on or near the downward extension of seismogenic faults and are accompanied by slow earthquakes there (Obara 2011). Therefore, the study of non-volcanic tremors is important for understanding processes leading to the generation of large earthquakes not only at the plate boundary but also in intraplate regions. Iio et al. (2004) proposed a model indicating that slip on a deeper extension of an active fault is required to generate large intraplate earthquakes. These observations suggest that locations and focal mechanisms of tremors near intraplate faults can provide clues to understanding the loading process responsible for earthquakes in intraplate regions.

Chao and Obara (Active triggered tremor sources in the inland fault systems of Japan, submitted) investigated the distribution of triggered tremors in Japan. One of the events described in their study occurred beneath the Hinagu fault zone, Kyushu, Japan. However, precise locations and focal mechanisms of these tremors have not yet been determined. Therefore, we performed a detailed analysis to estimate locations and focal mechanisms of these events from data of a dense seismic network deployed around the Hinagu fault zone and discuss a possible mechanism for the loading process leading to tectonic earthquakes.

Data, methods, and results

Tremor location in the Hinagu fault zone

In this study, we focused on tremors associated with seismic waves generated by the Sumatra earthquake (Mw 8.6; Meng et al. 2012) because these tremors were recorded with a relatively high signal-to-noise (S/N) ratio by a seismic network deployed on Kyushu Island, Japan. Permanent seismic observation stations had been installed around the source region by various organizations

* Correspondence: m.miyazaki_sevo@kyudai.jp
Institute of Seismology and Volcanology, Faculty of Sciences, Kyushu University, Shimabara 855-0843, Japan

Springer

© 2015 Miyazaki et al. **Open Access** This article is distributed under the terms of the Creative Commons Attribution 4.0 International License (http://creativecommons.org/licenses/by/4.0/), which permits unrestricted use, distribution, and reproduction in any medium, provided you give appropriate credit to the original author(s) and the source, provide a link to the Creative Commons license, and indicate if changes were made.

(Fig. 1). In addition, we deployed two temporal observation stations to determine precise locations and focal mechanisms of earthquakes in this area. Seismic records associated with the 2012 Sumatra earthquake are shown in Fig. 2, which shows that tremors occurred after the arrivals of Love waves. Tremors with large amplitudes (i.e., the events #3 and #5 in Fig. 2) can be identified during the arrivals of large surface waves in the original broadband records observed at "smt". We measured the peak intervals of the surface waves during the two large tremors and found that dominant periods of Love waves and Rayleigh waves were around 20 s and around 27 s, respectively. In this study, we analyzed five distinct tremors.

We estimated tremor locations using the method described in Chao et al. (2012). First, the horizontal components of waveforms at a station were bandpass-filtered between 2 and 8 Hz and then converted to mean-square (MS) envelopes. The envelope cross-correlation method developed by Obara (2002) was used to estimate differential travel times of station pairs. We only used the differential travel times with the higher cross-correlation coefficients (at least 0.65) as the reliable data. In addition, we excluded the data disturbed by artificial noises. The optimum hypocenter of a tremor was determined by a grid search. We calculated root-mean-square (RMS) differential travel time residuals for station pairs from an assumed grid point and searched a grid that provided minimum residuals among the distributed grid points. The grids were distributed at intervals of 0.2 km in the area shown in Fig. 3a at a depth range of 0–40 km. Theoretical S-wave travel times were calculated in a 1-D velocity model that was used to determine hypocenters of structural earthquakes by Kyushu University (Fig. 3c). We evaluated reliabilities of tremor locations using the bootstrap method (Efron 1979). Resampling of differential travel times was conducted 2000 times, and the 95 % bootstrap confidence interval was used as the estimation

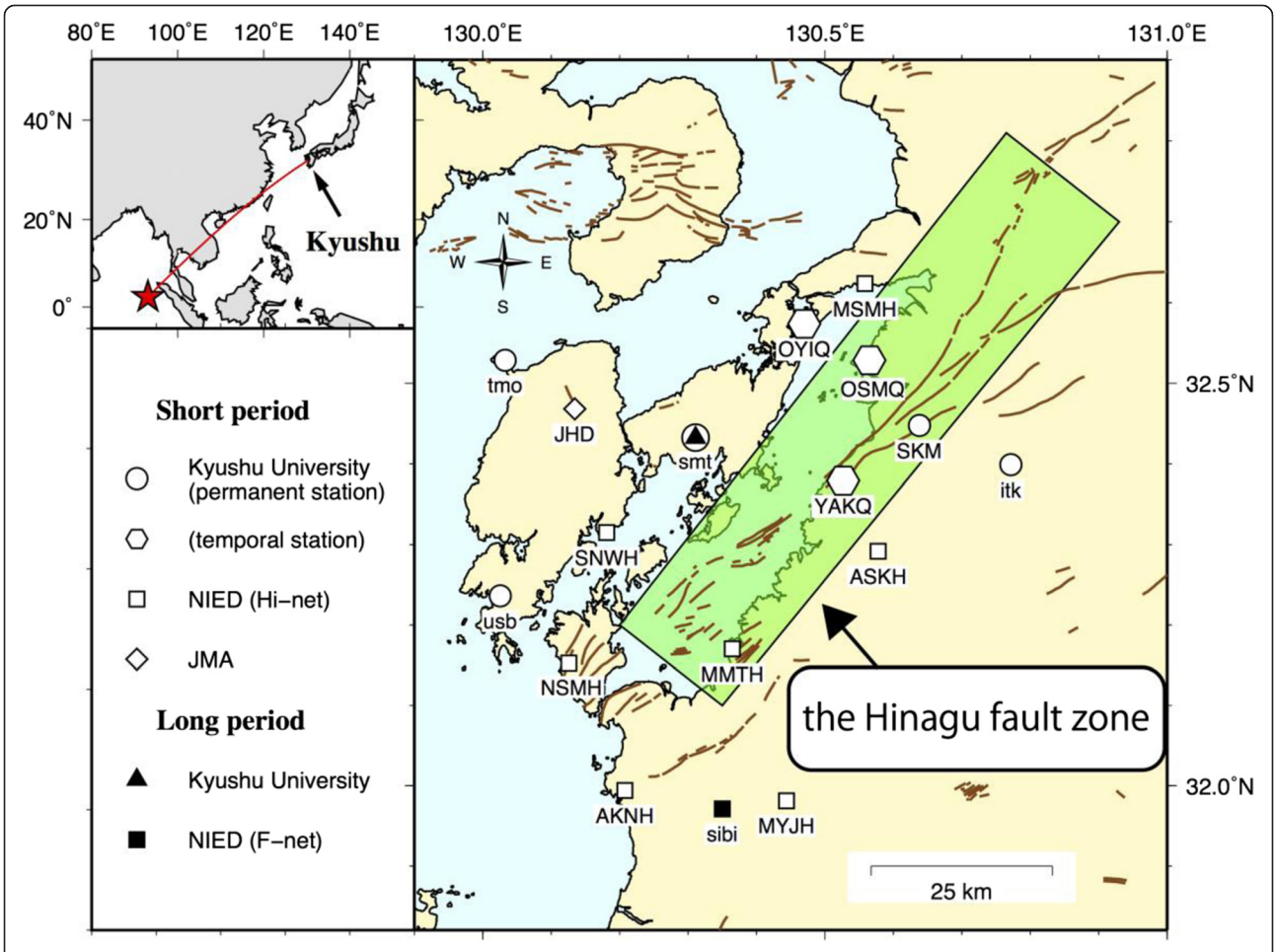

Fig. 1 Map view of the distribution of seismic stations around the Hinagu fault zone. Stations are indicated by *symbols* with *letter codes*. Stations installed by organizations are listed in the legend. The *red star* in the *upper left panel* denotes the epicenter of the 2012 Sumatra earthquake. *Brown lines* are surface traces of active faults. The *green-shaded area* shows the Hinagu fault zone. *NIED* National Research Institute for Earth Science and Disaster Prevention, *JMA* Japan Meteorological Agency

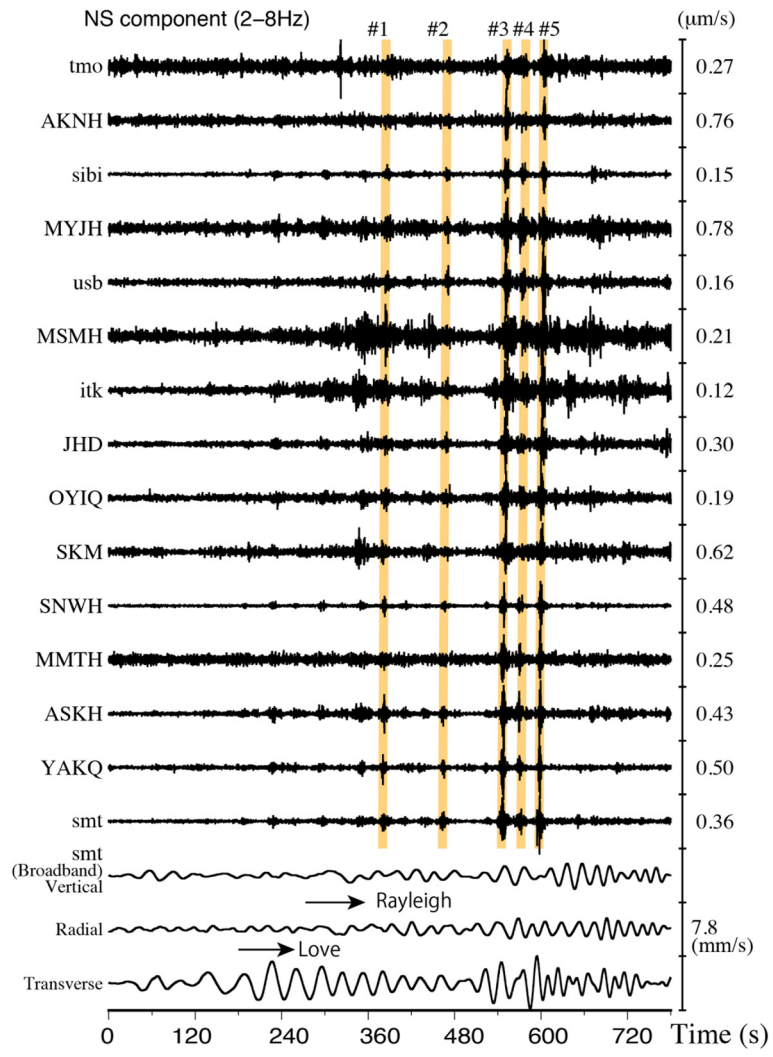

Fig. 2 Seismic records of the 2012 Sumatra earthquake recorded at the stations shown in Fig. 1. The top fifteen waveforms are the north-south (NS) components of bandpass-filtered seismograms (2–8 Hz). The bottom three traces are three components (vertical, radial, and transverse from the epicenter) recorded by the broadband seismometers installed at station "smt." *Orange lines* indicate the tremor signals analyzed in this study. The lapse time starts at 17:57 hours on 11 April 2012, in Japan Standard Time

error. The obtained locations of the tremors are shown in Fig. 3. The hypocenters of the tremors are located at a depth range between 18 and 23 km. The estimation error in the vertical direction was generally 2 km. The locations indicate that the tremors occurred beneath the fault zone.

Focal mechanism of the tremors

Analyses using propagation velocity (Obara 2002; Katsumata and Kamaya 2003), polarization (La Rocca et al. 2005, 2009; Wech and Creager 2007), and stacked waveform (Ide et al. 2007; Shelly et al. 2006, 2007) suggested that non-volcanic tremors consist of many overlapping S-waves radiating from low-frequency earthquakes (LFEs). The waveforms of each tremor investigated in this study are characterized by obscure phase arrivals and long durations, suggesting superposition of small events.

To estimate the focal mechanisms of such very small events, we utilized an S-wave polarization analysis because we could not adopt a prevalent moment tensor analysis to such small events. Here, we assumed that slip directions of small events are constant during the period of tremor generation and that the relative amplitude of the resultant waves is characterized by a radiation pattern from the source. Under this assumption, an S-wave polarization angle at a station during a tremor could be expected to have a certain direction corresponding to its focal mechanism. Although an influence of P-waves may not be absent (La Rocca et al. 2005; Ide et al. 2007), the waveform of the horizontal component of the

seismogram at the expected P-wave arrival does not reveal a distinct phase arrival. Therefore, we assumed that the contribution of P-waves to the seismogram was small enough to analyze a tremor as a single packet.

In this study, we attempted to estimate the S-wave polarization angle by extracting the directions of particle motion from waveforms during tremor events (#3 and #5 in Fig. 2) because these events had large enough amplitudes compared with the other events. According to Hirasawa (1970), the residual of the S-wave polarization angle (R) between observed (Γ) and theoretical S-wave polarization angle at the i-th station can be described as

$$R_i = \tan^{-1}\left(\frac{U_{SV}\sin\Gamma_i - U_{SH}\cos\Gamma_i}{U_{SV}\cos\Gamma_i + U_{SH}\sin\Gamma_i}\right), \quad (1)$$

where U_{SV} and U_{SH} are the amplitudes of the SV and SH components of S-waves, respectively. The residual R_i at i-th station are in a range $(-\pi/2, \pi/2)$. In this formula, U_{SV} and U_{SH} are functions of objective parameters (i.e., fault slip parameters of strike ϕ, dip δ, and rake λ angles) and takeoff angle and azimuth to the station from the hypocenter. The RMS residual (F) is calculated by summing residuals at all the stations used in this study with weighting factors (σ_i),

$$F(\phi,\delta,\lambda) = \sqrt{\frac{\sum_i^N (\sigma_i \cdot R_i^2)}{N}}, \quad (2)$$

where N is the number of stations used. A grid search is performed to find the optimal parameters for ϕ, δ, and λ that minimize the function F. The definition of σ_i is described below. In this study, we used the 15 stations deployed around the hypocentral area of the tremors.

We determined directions of particle motion as follows, with the diagram for the station "YAKQ" shown in Fig. 4 serving as an example. Firstly, we applied a bandpass filter in the frequency range of 2 to 8 Hz to three-component velocity seismograms (Fig. 4a). A polarization analysis of waveform within a moving time

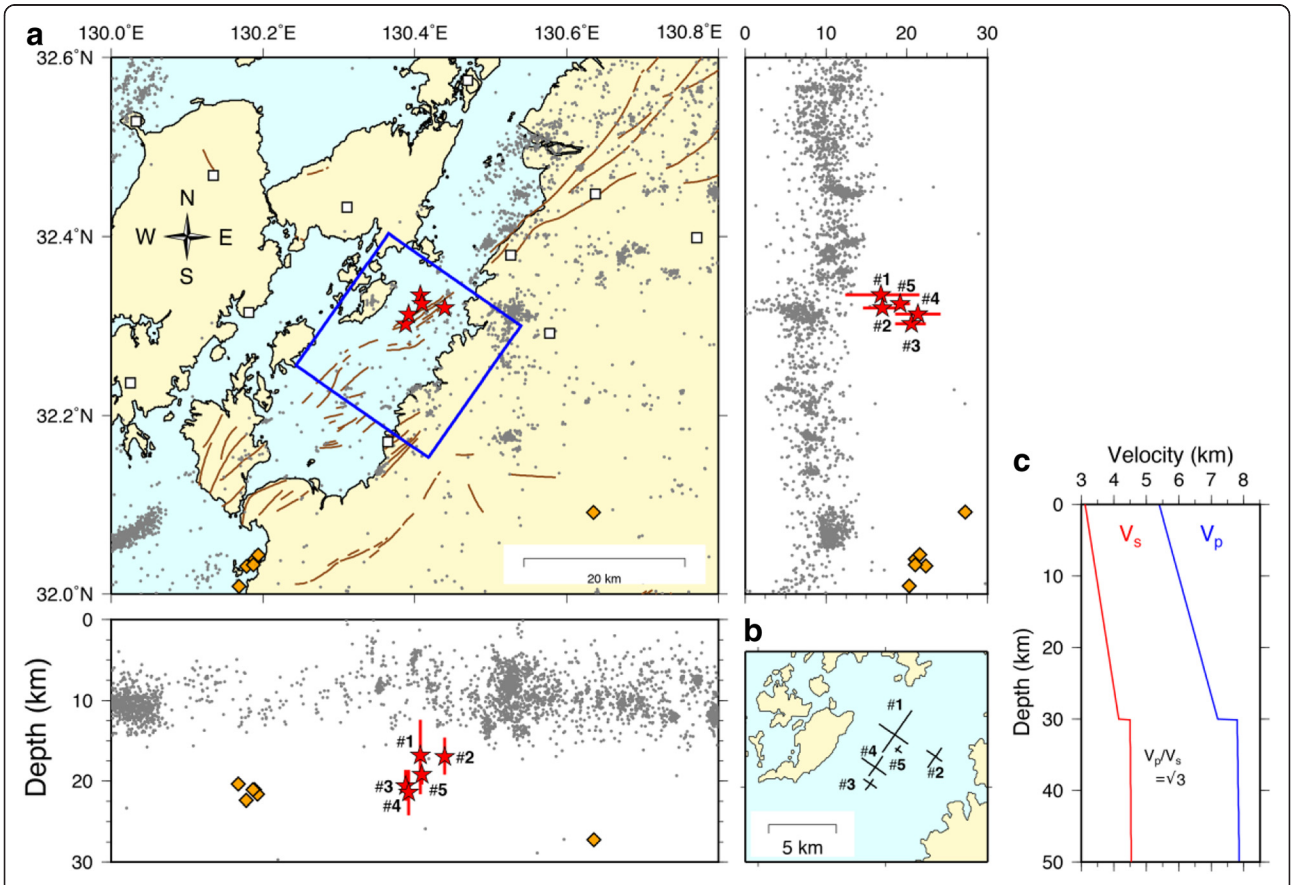

Fig. 3 **a** Map view and vertical cross sections in N-S and E-W directions for the estimated tremor locations (*red stars*) and regular earthquakes (*gray dots*) that occurred during 2010–2013. *Red bars* in cross sections denote the 95 % bootstrap confidence intervals in the vertical direction. The *blue rectangle* shows the grid search area for hypocenter determination of the tremors with a size of 20 km horizontally and 40 km vertically. *Orange diamonds* are LFE events identified by JMA. **b** Map showing the 95 % bootstrap confidence intervals of the horizontal tremor locations. **c** Velocity structures used in this study

window of 0.5 s during a lapse time was performed. The direction of particle motion in each time window (open circles in Fig. 4b) is defined as the horizontal direction of eigenvectors of particle ground velocities with the maximum eigenvalue. Directions of the maximum eigenvector vary with time-lapse windows, suggesting that the seismic signals are affected by background noise. Therefore, we set two conditions to extract reliable data. One is a rectilinearity (Nuttli 1961, Chouet et al. 1997) of the particle ground velocity, which can be described as

$$\frac{w_3}{\sqrt{w_1^2 + w_2^2 + w_3^2}} \quad , \tag{3}$$

where w_1,w_2, and w_3 are minimum, moderate, and maximum eigenvalues in each time window, respectively. We extracted the data under the condition that the rectilinearity was higher than 0.9 (black line in Fig. 4c). The other criterion is that the signal-to-noise ratio was larger than 2.5 (red line in Fig. 4c). The amplitude of the signal is calculated from the waveform within the time window of 0.5 s used in the polarization analysis. The amplitude of the noise is defined as the RMS amplitude within a time window of 10 min that contains both the tremor signals and ambient noises.

After selection of the data (blue circles in Fig. 4b), we obtained the azimuthal distribution of the directions of particle motions within the target lapse time range for each station (blue bars in Fig. 4d). To evaluate the stability in the azimuthal direction, we counted the cumulative frequency of the azimuthal distribution for every ±2° in the azimuthal range. The frequency distribution was normalized by the total number of samples (orange line in Fig. 4d). Finally, we obtained the observed S polarization angle as the angular difference between the azimuthal direction with the maximum relative frequency (orange line in Fig. 4b, e) and the direction from each station toward the epicenter (red line in Fig. 4b, e). We used the value of the maximum relative frequency as the weighting factor (σ_i) for the following grid search. Even if several peaks emerged in the smoothed azimuthal distribution, the influence on the focal mechanism estimation was restrained because the weighting factor became small in that case.

In this study, we neglected the polarity of the particle motion because we did not recognize clear phase onsets (Fig. 4). Therefore, only the nodal planes could be

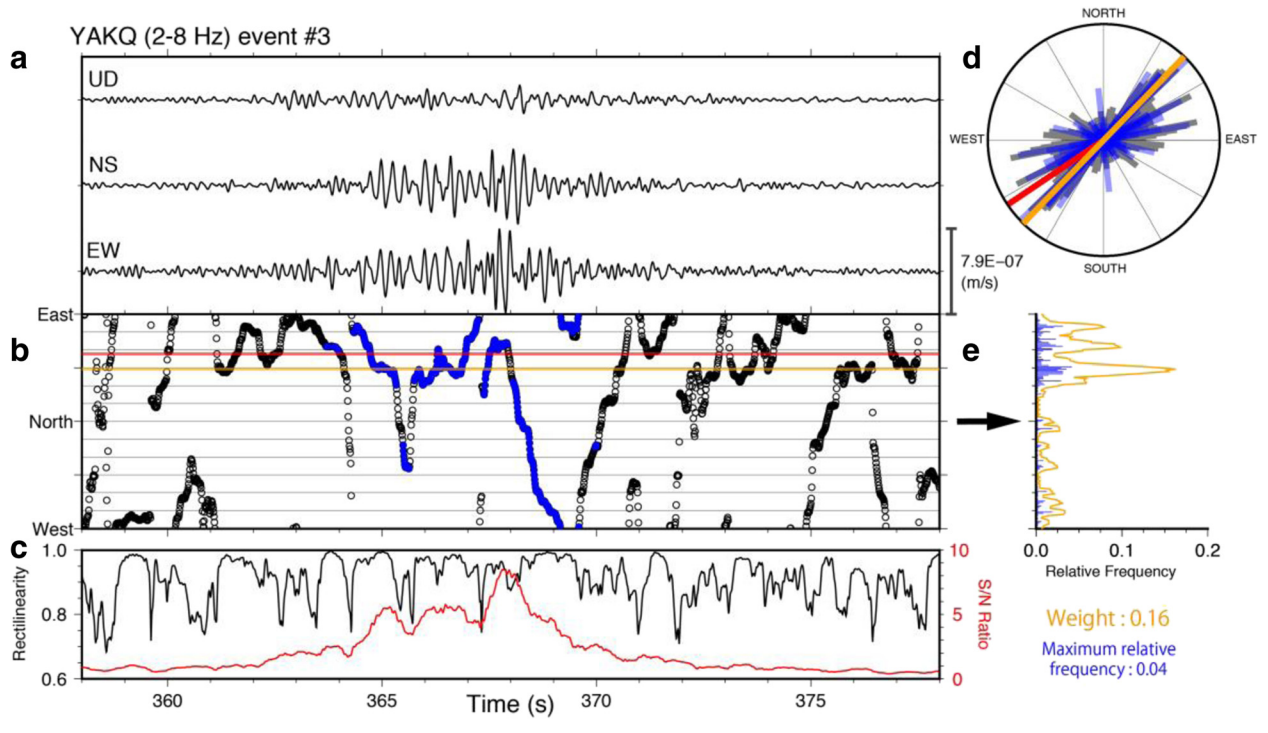

Fig. 4 An example of our polarization analysis. **a** Three-component seismograms observed at station "YAKQ", bandpass-filtered at 2–8 Hz. **b** Directions of particle velocity motion (*open circles*). *Blue circles* represent extracted data with high rectilinearity and S/N ratios. **c** Rectilinearity (*black line*) and signal-to-noise ratio (*red line*). **d** Azimuthal projection of cumulative numbers of the determined polarization directions. *Blue* and *gray segments* indicate extracted data and other data, respectively. *Red* and *orange bars* denote the azimuth toward the epicenter and the estimated polarized direction, respectively. **e** Same as **d**, except for plotting the azimuth parallel to **b**. *Orange line* in Fig. 4e indicates the cumulative number of the polarization directions for azimuthal fractions at a 2° interval

obtained by the above estimation, and P and T axes of the obtained solutions can substitute for each other. We set a 1° grid for each parameter range of $0° \le \phi < 360°$ ($\phi = 0°$ means North and ϕ increases in clockwise direction), $0° \le \delta \le 90°$ and $0° \le \lambda < 180°$. The obtained results are shown in Fig. 5. Two fault planes and the directions of the P or T axes are plotted. To check the local minima, we investigated the distribution of both axes for which residuals were within +10 % from the minimal values, as shown in Fig. 5.

Discussions and conclusions

In this study, we estimated the locations and focal mechanisms of the triggered tremors in the Hinagu active fault zone. We found that five tremors were located beneath the seismogenic zone and seem to align the strike direction of the fault. These results suggest that the tremors occurred near the deeper extension of the Hinagu fault zone. The Japan Meteorological Agency detected low-frequency events around the Hinagu fault zone in 2004 and 2005 (Fig. 3). However, they were not triggered by the surface wave arrivals shown in this study and were located far from the tremors, and therefore, it is assumed that these events were not related to the tremors.

We estimated the focal mechanisms from the waveforms of two tremors with large amplitudes. Locations of P and T axes on the focal sphere are similar for these events, although some local minima were seen in the mechanism solution of the event #5. It can be seen in Fig. 5 that either the P or the T axis is oriented in a NW-SE direction. Although P and T axes of the obtained focal mechanisms can substitute for each other due to the polarization analysis in this study, the nodal planes are similar to those for the shallow earthquakes shown in Fig. 6a. Furthermore, a block inversion of geodetic data (Nishimura 2014) suggests that the downward extension of the Hinagu fault slips in the same direction as the seismogenic fault. Thus, it is likely that P and T axes of the obtained focal mechanisms of the tremors are similar to those of shallow earthquakes.

Therefore, we can compare the two optimal focal mechanisms of the tremors to the focal mechanisms of shallow crustal earthquakes studied by Matsumoto et al. (2013). We found that one of the nodal planes has a similar strike angle to that of the shallow earthquakes. Considering the principal stress directions estimated by Matsumoto et al. (2013) shown in Fig. 6a, the similar nodal planes of the tremors and crustal earthquakes are favorably oriented under the current stress field. This could imply that both the shallow earthquakes and the tremors in this region are generated under the same tectonic stress conditions. In addition, the Hinagu fault zone at the surface has similar strike direction to one of the nodal planes of optimal focal mechanisms estimated in this study. This implies the possibility that the tremors occurred on a fault plane forming a downward extension of the Hinagu fault zone. The similarity of strike angles of the fault planes suggests that the active fault, the shallow earthquakes, and the tremors represent a fault system reaching from the surface to the lower crust as described in Iio et al. (2004). This geometrical relationship indicates that the tremors are a

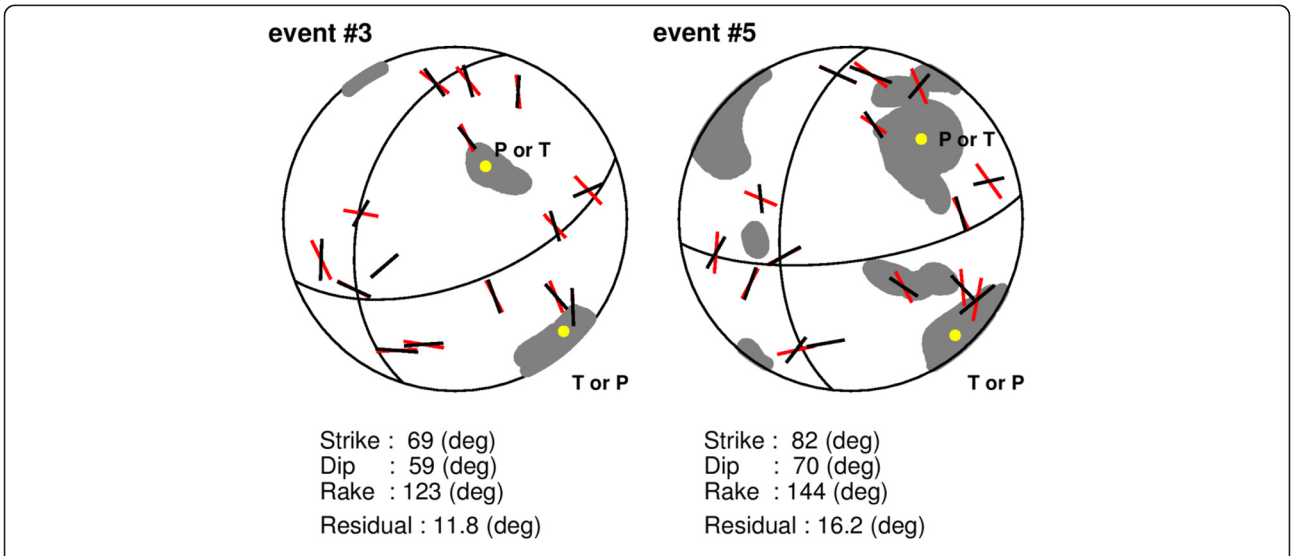

Fig. 5 Solutions of focal mechanisms with minimum residuals for each event. For each solution, estimated parameters (strike, dip, rake) and RMS residuals of polarization angle differences are listed. *Yellow circles* denote the P and T axes. *Black* and *red bars* denote the observed and theoretical polarization directions, respectively. *Gray-shaded areas* represent the locations of P or T axes that have residuals within +10 % from the best solutions

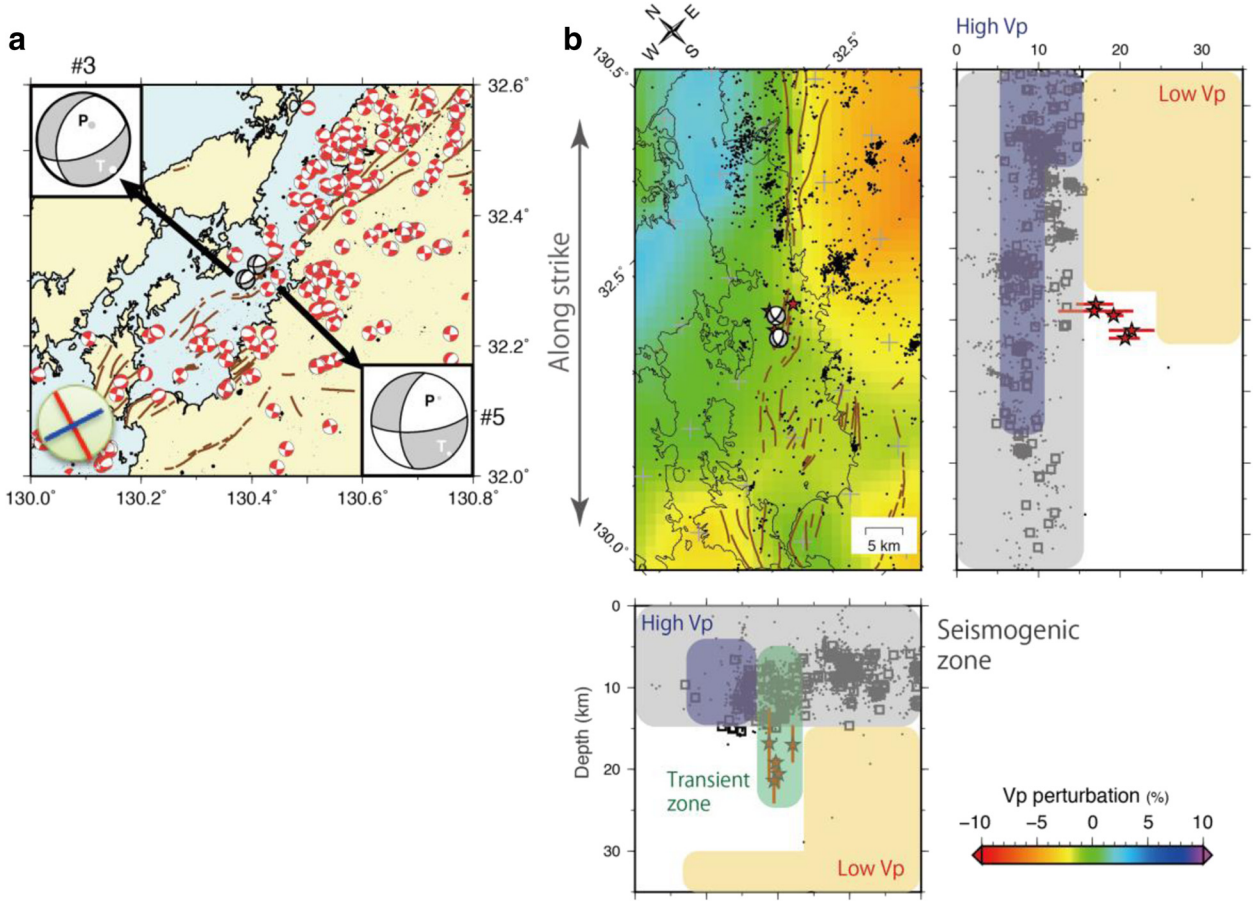

Fig. 6 a Map of estimated focal mechanisms. *Red-colored beach balls* show shallow earthquakes. The *gray-colored beach balls* represent the solutions of triggered tremors with minimum residuals. *Brown lines* are the same as in Fig. 1. *Red* and *blue segments* in the map indicate minimum and maximum principal stress directions projected in the horizontal plain derived from the focal mechanisms of shallow earthquakes, respectively (Matsumoto et al. 2013). **b** Map of Vp perturbations at 20-km depth and schematic illustration of the spatial variation of Vp in the cross sections (Matsubara and Obara 2011). *Red stars* and *bars* are the same as in Fig. 3. The depth distributions of shallow earthquakes that their focal mechanisms were plotted in Fig. 6a were marked as *black squares* in the subplots. *Black dots* in both figures denote the earthquakes that occurred during 2010–2013 (same as in Fig. 3)

phenomenon reflecting the loading process of the crustal earthquakes.

We also investigated the relationship between the locations of the tremors and the velocity structure (Fig. 6b), estimated by seismic tomographic inversion (Matsubara and Obara 2011). In the seismogenic zone, a region characterized by high P-wave velocities (Vp) exists parallel to the strike direction of the Hinagu fault zone. A low Vp region is seen below the tremor zone and in the northeastern part of the fault zone. The distribution of the tremors seems to indicate the possibility that the tremor is triggered in the transient zone between the seismogenic zone and the ductile lower crust.

In the Nankai trough region, Shelly et al. (2006) showed that the Vp/Vs ratio around the tremor source was over 1.8, which was interpreted as the existence of high pore-fluid pressure. This is also supported by the relationship between the volumetric strain change generated by surface waves and amplitudes of triggered tremors (Miyazawa and Brodsky 2008). Thomas et al. (2012) showed that high pore-fluid pressure exists in the brittle-ductile transient zone of a transform boundary in California via a study of tidal triggering of tectonic tremors. In contrast, the Vp/Vs ratio near the source region of the Hinagu fault is approximately 1.7 to 1.8 and seems to be less influenced by the fluid pressure. According to Matsubara and Obara (2011), the resolution of the velocity structure in the horizontal direction is 20 km. Therefore, there is a possibility that a high Vp/Vs region indicating high pore-pressure is concentrated in a limited region, smaller than the resolution of the velocity tomography.

Competing interests
The authors declare that they have no competing interests.

Authors' contributions
MM carried out the data processing and drafted the manuscript. SM and HS maintained the seismic stations and helped draft the manuscript. All authors read and approved the manuscript.

Acknowledgements
We are thankful to two anonymous reviewers for useful comments and suggestions to improve this manuscript. In this study, we used the seismic observation data recorded by various organizations, including the Japan Meteorological Agency (JMA), National Research Institute for Earth Science and Disaster Prevention (NIED), and Kagoshima University. Figures are generated by Generic Mapping Tools.

Received: 12 August 2015 Accepted: 22 October 2015
Published online: 04 November 2015

References

Chao K, Peng Z, Wu C, Tang C, Lin C (2012) Remote triggering of non-volcanic tremor around Taiwan. Geophys J Int 188:301–324. doi:10.1111/j.1365-246X.2011.05261.x
Chouet B, Saccorotti G, Martini M, Dawson P, DeLuca G, Milana G, Scarpa R (1997) Source and path effects in the wave fields of tremor and explosions at Stromboli Volcano, Italy. J Geophys Res. doi:10.1029/97JB00953.
Efron B (1979) Bootstrap methods: another look at the jackknife. Ann Statist 7:1–26. doi:10.1214/aos/1176344552
Hirasawa T (1970) Focal mechanism determination from S wave observations of different quality. J Phys Earth 18:285–294. doi:10.4294/jpe1952.18.285
Ide S, Shelly DR, Beroza GC (2007) Mechanism of deep low frequency earthquakes: further evidence that deep non-volcanic tremor is generated by shear slip on the plate interface. Geophys Res Lett. doi:10.1029/2006GL028890
Iio Y, Sagiya T, Kobayashi Y (2004) Origin of the concentrated deformation zone in the Japanese Islands and stress accumulation process of intraplate earthquakes. Earth, Planets and Space 56:831–42. doi:10.1186/BF03353090
Katsumata A, Kamaya N (2003) Low-frequency continuous tremor around the Moho discontinuity away from volcanoes in the southwest Japan. Geophys Res Lett. doi:10.1029/2002GL015981.
Kita S, Nakajima J, Hasegawa A, Okada T, Katsumata K, Asano Y, Kimura T (2014) Detailed seismic attenuation structure beneath Hokkaido, northeastern Japan: arc-arc collision process, arc magmatism, and seismotectonics. J Geophys Res. doi:10.1002/2014JB011099.
La Rocca M, McCausland W, Galluzzo D, Malone S, Saccorotti G, Pezzo ED (2005) Array measurements of deep tremor signals in the Cascadia subduction zone. Geophys Res Lett. doi:10.1029/2005GL023974.
La Rocca M, Creager KC, Galluzzo D, Malone S, Vidale JE, Sweet JR, Wech AG (2009) Cascadia tremor located near plate interface constrained by S minus P wave times. Science 323:620–3. doi:10.1126/science.1167112
Matsubara M, Obara K (2011) The 2011 off the Pacific coast of Tohoku Earthquake related to a strong velocity gradient with the Pacific plate. Earth, Planets and Space 63:663–7. doi:10.5047/eps.2011.05.018
Matsumoto S, Chikura H, Ohkura T, Miyazaki M, Shimizu H, Abe Y, Inoue H, Yoshikawa S, Yamashita Y (2013) Spatial heterogeneities of deviatoric stress and pore-pressure in Kyushu, Japan, and their implication for seismic activity. In: EGU general assembly 2013, Vienna, Austria, 7-12 April 2013. http://meetingorganizer.copernicus.org/EGU2013/posters/12580
Meng L, Ampuero JP, Stock J, Duputel Z, Luo Y, Tsai VC (2012) An earthquake in a maze: compressional rupture branching during the 2012 Mw8.6 Sumatra earthquake. Science 337:724–6. doi:10.1126/science.1224030
Miyazawa M, Brodsky EE (2008) Deep low-frequency tremor that correlates with passing surface waves. J Geophys Res. doi:10.1029/2006JB004890.
Nishimura T (2014) Crustal block movements of southwestern Japan estimated by fault-block modeling of GNSS data (In Japanese). In: Programme and Abstracts, the Seismological Society of Japan, 2014, fall meeting, Seismological Society of Japan, Niigata, Japan, 24-26 November 2014
Nuttli O (1961) The effect of the Earth's surface on the S wave particle motion. Bull Seismol Soc Am 51:237–46
Obara K (2002) Nonvolcanic deep tremor associated with subduction in southwest Japan. Science 296:1679–81. doi:10.1126/science.1070378
Obara K (2011) Characteristics and interactions between non-volcanic tremor and related slow earthquakes in the Nankai subduction zone, southwest Japan. J Geodyn 52:229–48. doi:10.1016/j.jog.2011.04.002
Obara K (2012) New detection of tremor triggered in Hokkaido, northern Japan by the 2004 Sumatra-Andaman earthquake. Geophys Res Lett. doi:10.1029/2012GL053339.
Peng Z, Vidale JE, Wech AG, Nadeau RM, Creager KC (2009) Remote triggering of tremor along the San Andreas Fault in central California. J Geophys Res. doi:10.1029/2008JB006049.
Rubinstein JL, Gomberg J, Vidale JE, Wech AG, Kao H, Creager KC, Rogers G (2009) Seismic wave triggering of nonvolcanic tremor, episodic tremor and slip, and earthquakes on Vancouver Island. J Geophys Res. doi:10.1029/2008JB005875.
Shelly DR, Beroza GC, Ide S, Nakamula S (2006) Low-frequency earthquakes in Shikoku, Japan, and their relationship to episodic tremor and slip. Nature 442:188–191. doi:10.1038/nature04931
Shelly DR, Beroza GC, Ide S (2007) Non-volcanic tremor and low-frequency earthquake swarms. Nature 446:305–307. doi:10.1038/nature05666
Thomas AM, Bürgmann R, Shelly DR, Beeler NM, Rudolph ML (2012) Tidal triggering of low frequency earthquakes near Parkfield, California: implications for fault mechanics within the brittle-ductile transition. J Geophys Res. doi:10.1029/2011JB009036.
Wech AG, Creager KC (2007) Cascadia tremor polarization evidence for plate interface slip. Geophys Res Lett. doi:10.1029/2007GL031167.
Yabe S, Ide S (2013) Repeating deep tremors on the plate interface beneath Kyushu, southwest Japan. Earth, Planets Space 65:17–23. doi:10.5047/eps.2012.06.001

Submit your manuscript to a SpringerOpen journal and benefit from:

► Convenient online submission
► Rigorous peer review
► Immediate publication on acceptance
► Open access: articles freely available online
► High visibility within the field
► Retaining the copyright to your article

Submit your next manuscript at ► springeropen.com